

## Methods

### Slice preparation and two-photon imaging

Slices (thickness, 300–350  $\mu\text{m}$ ) were prepared from visual cortices of P14–21 C57BL/6 mice using a Leica VT 1000S tissue slicer with ice-cold oxygenated modified aCSF that included 0.5 mM  $\text{CaCl}_2$  and 7 mM  $\text{MgSO}_4$ , in which NaCl was replaced by an equimolar concentration of sucrose. For AM-loading, slices were incubated in a small vial containing 2.5 ml of oxygenated aCSF with 25  $\mu\text{l}$  of a 1 mM Fura2-AM solution (Molecular Probes; in 100% dimethylsulphoxide) for 20–30 min. Slices were incubated in the dark, and the incubation solution was maintained at 35–37 °C. Experiments were performed at 35–37 °C with aCSF containing (in mM) 123 NaCl, 3 KCl, 26  $\text{NaHCO}_3$ , 1  $\text{NaH}_2\text{PO}_4$ , 2  $\text{CaCl}_2$ , 2  $\text{MgSO}_4$  and 10 dextrose, which was continuously aerated with 95%  $\text{O}_2$ , 5%  $\text{CO}_2$ . Imaging was carried out with a custom-made two-photon laser scanning microscope<sup>28</sup> consisting of a modified Fluoview (Olympus) confocal microscope with a Mira Ti:sapphire laser (Coherent) providing 130 fs pulses at 75 MHz, pumped by a solid-state source (Verdi, Coherent). Slices were imaged using a low-magnification, high-numerical-aperture objective ( $\times 20$ , NA-0.95, Olympus). Frames were acquired at 0.9–1.6 s per frame. The size of the imaged field was typically  $\sim 400 \times 700 \mu\text{m}$ .

### Electrophysiology

Cells were held in current clamp using a patch-clamp amplifier (BVC-700, Dagan Corporation). Pipette solution contained 130 mM potassium methylsulphate, 5 mM KCl, 5 mM NaCl, 10 mM HEPES, 2.5 mM Mg-ATP, 0.3 mM GTP, 30  $\mu\text{M}$  Fura-2 pentapotassium salt (Molecular Probes) and 0.5% biocytin. The osmolarity was 265–275 mosM, pH 7.3. Microelectrodes had a resistance of 4–10 M $\Omega$ . Recordings were digitized online (10 kHz) with an A/D board (Instrutech) and analysed offline with MiniAnalysis 5.1 (Synaptosoft, Inc.). Neurons were filled with biocytin during recording and processed for morphological identification.

AMPA receptors were blocked by 6-cyano-7-nitroquinoxaline-2,3-dione (CNQX; 10  $\mu\text{M}$ ), 6,7-dinitro-2,3-quinoxalinedione (DNQX; 10  $\mu\text{M}$ ) or NBQX (10  $\mu\text{M}$ ). NMDA receptors were blocked by D-2-amino-5-phosphonopentanoate (AP5; 40  $\mu\text{M}$ ) or MK801 (10  $\mu\text{M}$ ). As we did not observe any significant differences in the effects of these antagonists, the data were pooled for further analysis. CNQX, DNQX, NBQX, picrotoxin and AP5 were purchased from Sigma; MK801 was obtained from Tocris.

### Analysis

Online analysis was performed with custom-made software in ImageJ (National Institutes of Health) and Matlab (MathWorks). To detect calcium signals from imaged cells, we automatically identified loaded entities in images of the slices, and measured the average fluorescence of these entities as a function of time. To detect individual optical events, the baseline of each trace was calculated by smoothing the trace with a high-order Hanning filter (window length, 6–7 s). We estimated the amount of noise by subtracting the baseline from the trace and measuring the standard deviation of the values of all points above the baseline. We then divided the trace by this noise level to normalize it, and considered the threshold of 1 unit below the baseline. Five action potentials were usually necessary to produce a calcium transient of this magnitude. Event times were marked at the local minima of the trace that occurred below the threshold level (Fig. 1c).

To identify peaks of synchronous activity that included more cells than expected by chance, we used interval reshuffling (randomly reordering of intervals between events for each cell) to create sets of surrogate event sequences<sup>12</sup>. Reshuffling was carried out 1,000 times for each movie, and a surrogate histogram was constructed for each reshuffling. The threshold corresponding to a significance level of  $P < 0.05$  was estimated as the number of coactive cells exceeded in a single frame in only 5% of these histograms. We then examined each peak that was significant at  $P < 0.05$ , and manually rejected traces where noise was erroneously detected as an event. Peaks of synchronous activity that remained significant were selected for further analysis. For each peak of synchrony, we sought to determine whether the arrangement of cells involved could be classified into one of three spatial patterns (clusters, layers or columns) with confidence. We characterized each pattern of coactive cells by three measurements: the average distance between cell locations and their centroid, the average length of the projections of these distances in the direction parallel to the pia, and the average length of the projections in the direction perpendicular to the pia. For each pattern, we created 1,000 surrogate arrangements of cells using Monte Carlo simulations, choosing the same number of cells at random from the slice each time. All three measurements were made for each of the surrogate patterns, and the significance of the spatial arrangement was determined by directly comparing the resulting distributions with the original measurements. If distance projections were significantly small ( $P < 0.05$ ) only in the direction parallel or perpendicular to the pia, the pattern was classified as a column or a layer, respectively. If the unprojected distances were significantly small, the pattern was classified as a cluster.

Received 16 December 2002; accepted 25 March 2003; doi:10.1038/nature01614.

1. Mountcastle, V. B. *Perceptual Neuroscience: The Cerebral Cortex* (Harvard Univ. Press, Cambridge, Massachusetts, 1998).
2. Hubel, D. H. & Wiesel, T. N. Functional architecture of the macaque monkey visual cortex. *Proc. R. Soc. Lond. B* **198**, 1–59 (1977).
3. Lorente de Nó, R. Analysis of the activity of the chains of internuncial neurons. *J. Neurophysiol.* **1**, 207–244 (1938).
4. Gilbert, C. & Wiesel, T. N. Morphology and intracortical projections of functionally characterised neurons in the cat visual cortex. *Nature* **280**, 120–125 (1979).
5. Douglas, R. J. & Martin, K. A. C. In *The Synaptic Organization of the Brain* (ed. Shepherd, G. M.) 459–511 (Oxford Univ. Press, Oxford, 1998).

6. Somogyi, P., Tamas, G., Lujan, R. & Buhl, E. Salient features of synaptic organisation in the cerebral cortex. *Brain Res. Brain Res. Rev.* **26**, 113–135 (1998).
7. Llinás, R. *I of the Vortex: From Neurons to Self* (MIT Press, Cambridge, Massachusetts, 2002).
8. Creutzfeldt, O. *Cortex Cerebri* (Oxford Univ. Press, Oxford, 1995).
9. Steriade, M., Contreras, D., Curro, D. R. & Nunez, A. The slow (<1 Hz) oscillation in reticular thalamic and thalamocortical neurons: scenario of sleep rhythm generation in interacting thalamic and neocortical networks. *J. Neurosci.* **13**, 3284–3299 (1993).
10. Todyks, M., Kenet, T., Grinvald, A. & Arieli, A. Linking spontaneous activity of single cortical neurons and the underlying functional architecture. *Science* **286**, 1943–1946 (1999).
11. Sanchez-Vives, M. & McCormick, D. Cellular and network mechanisms of rhythmic recurrent activity in neocortex. *Nature Neurosci.* **3**, 1027–1034 (2000).
12. Mao, B. Q., Hamzei-Sichani, F., Aronov, D., Froemke, R. C. & Yuste, R. Dynamics of spontaneous activity in neocortical slices. *Neuron* **32**, 883–898 (2001).
13. Wilson, C. J. & Groves, P. M. Spontaneous firing patterns of identified spiny neurons in the rat neostriatum. *Brain Res.* **220**, 67–80 (1981).
14. Cowan, R. L. & Wilson, C. J. Spontaneous firing patterns and axonal projections of single corticostriatal neurons in the rat medial agranular cortex. *J. Neurophysiol.* **71**, 17–32 (1994).
15. Steriade, M., Nuñez, A. & Amzica, F. A novel slow (~1 Hz) oscillation of neocortical neurons *in vivo*: depolarizing and hyperpolarizing components. *J. Neurosci.* **13**, 3252–3265 (1993).
16. Anderson, J., Lampl, I., Reichova, I., Carandini, M. & Ferster, D. Stimulus dependence of two-state fluctuations of membrane potential in cat visual cortex. *Nature Neurosci.* **3**, 617–621 (2000).
17. Fuster, J. M. The prefrontal cortex and its relation to behavior. *Prog. Brain Res.* **87**, 201–211 (1997).
18. Goldman-Rakic, P. S. Cellular basis of working memory. *Neuron* **14**, 477–485 (1995).
19. Durstewitz, D., Seamans, J. K. & Sejnowski, T. J. Neurocomputational models of working memory. *Nature Neurosci.* **3** suppl., 1184–1191 (2000).
20. Wang, X. J. Synaptic reverberation underlying mnemonic persistent activity. *Trends Neurosci.* **24**, 455–463 (2001).
21. Seung, H. S., Lee, D. D., Reis, B. Y. & Tank, D. W. Stability of the memory of eye position in a recurrent network of conductance-based model neurons. *Neuron* **26**, 259–271 (2000).
22. Hopfield, J. J. Neural networks and physical systems with emergent collective computational abilities. *Proc. Natl Acad. Sci. USA* **79**, 2554–2558 (1982).
23. Badea, T., Goldberg, J., Mao, B. Q. & Yuste, R. Calcium imaging of epileptiform events with single-cell resolution. *J. Neurobiol.* **48**, 215–227 (2001).
24. Shu, Y., Hasenstaub, A. & McCormick, D. A. Turning on and off recurrent balanced cortical activity. *Nature* **423**, 288–293 (2003).
25. Constantinidis, C., Franowicz, M. & Goldman-Rakic, P. Coding specificity in cortical microcircuits: a multiple-electrode analysis of primate prefrontal cortex. *J. Neurosci.* **21**, 3646–3655 (2001).
26. Ben-Yishai, R., Lev Bar-Or, R. & Sompolinsky, H. Orientation tuning by recurrent neural networks in visual cortex. *Proc. Natl Acad. Sci. USA* **92**, 3844–3848 (1995).
27. Hebb, D. O. *The Organization of Behaviour* (Wiley, New York, 1949).
28. Majewska, A., Yiu, G. & Yuste, R. A custom-made two-photon microscope and deconvolution system. *Pflugers Arch.* **441**, 398–409 (2000).

Supplementary Information accompanies the paper on [www.nature.com/nature](http://www.nature.com/nature).

**Acknowledgements** We thank D. McCormick for advice as well as J. Hopfield and members of our laboratory for comments. Supported by NEI, NINDS, FRM, the Human Frontier Science Program, the New York STAR Center for High Resolution Imaging of Functional Neural Circuits and the John Merck Fund.

**Competing interests statement** The authors declare that they have no competing financial interests.

**Correspondence** and requests for materials should be addressed to R.C. (rcossart@biology.columbia.edu).

## Turning on and off recurrent balanced cortical activity

Yousheng Shu, Andrea Hasenstaub & David A. McCormick

Department of Neurobiology, Yale University School of Medicine, 333 Cedar Street, New Haven, Connecticut 06510, USA

The vast majority of synaptic connections onto neurons in the cerebral cortex arise from other cortical neurons, both excitatory and inhibitory, forming local and distant ‘recurrent’ networks. Although this is a basic theme of cortical organization, its study has been limited largely to theoretical investigations, which predict that local recurrent networks show a proportionality or balance between recurrent excitation and inhibition, allowing the generation of stable periods of activity<sup>1–5</sup>. This recurrent activity might underlie such diverse operations as short-term

memory<sup>4,6,7</sup>, the modulation of neuronal excitability with attention<sup>8,9</sup>, and the generation of spontaneous activity during sleep<sup>5,10–14</sup>. Here we show that local cortical circuits do indeed operate through a proportional balance of excitation and inhibition generated through local recurrent connections, and that the operation of such circuits can generate self-sustaining activity that can be turned on and off by synaptic inputs. These results confirm the long-hypothesized role of recurrent activity as a basic operation of the cerebral cortex.

Maintaining slices of ferret prefrontal and occipital cortex *in vitro* resulted in the spontaneous and periodic (once every 3–7 s) generation of synaptic and action potential activity for periods of 1–3 s in cells recorded from layers II–VI (Fig. 1a); this activity was initiated earliest and most intensely in layer V<sup>13</sup>. Extracellular recordings from single layer-V neurons revealed that during the period of neuronal activity (the ‘UP’ state), these cells fired between 2 and 47 Hz (mean,  $17.1 \pm 11.1$  Hz;  $n = 32$ ). During the periods of relative quiescence (the ‘DOWN’ state), 18 of these cells did not discharge spontaneously, whereas the other 14 discharged at an average rate of  $3.6 \pm 3.0$  Hz. These alternating UP and DOWN states, which are characterized by the participation of every neuron recorded, closely resemble those occurring *in vivo* during slow-wave sleep and anaesthesia<sup>10–14</sup>. Intracellularly, each UP state *in vitro* was associated with a square or trapezoid-shaped 4–10-mV depolarization of pyramidal neurons and fast-spiking (FS) interneurons in synchrony with nearby multiple-unit activity (Fig. 1). The sustained activity of the UP state was shown to be generated through network mechanisms, as it was associated with large barrages of synaptic potentials, and because preventing the generation of action potentials by hyperpolarizing the neuron by 10–30 mV did not affect the duration of the UP state (normal,  $1.7 \pm 0.3$  s; hyperpolarized,  $1.7 \pm 0.4$  s;  $n = 16$  cells) or its rate of recurrence (normal,  $0.2 \pm 0.1$  Hz; hyperpolarized,  $0.2 \pm 0.1$  Hz), as has also been observed *in vivo*<sup>10–14</sup>. Bath application of the non-NMDA (*N*-methyl-D-aspartate) glutamate ionotropic receptor antagonist 6-cyano-7-nitroquinoxaline-2,3-dione (CNQX; 5–10  $\mu$ M;  $n = 8$ ) or the NMDA receptor antagonist DL-2-amino-5-phosphonopentanoate (DL-AP5; 10–25  $\mu$ M;  $n = 7$ ) completely blocked the generation of recurrent activity in extracellular multiple-unit recordings, although a minority of neurons continued to exhibit low-level spontaneous action potential activity (not shown; see ref. 5). Block of GABA<sub>A</sub> ( $\gamma$ -aminobutyric acid type A) receptors with bath-applied picrotoxin (50  $\mu$ M;  $n = 8$ ) transformed slow oscillations into seizure-like activity<sup>13</sup> (see Supplementary Information; for more information, see <http://www.mccormicklab.org>).

Depolarizing current pulses did not result in the generation of ‘after discharges’ in single cortical neurons ( $n = 25$ ), as has been observed following the artificial stimulation of muscarinic receptors<sup>15</sup>. Moreover, the interspike intervals of regular-spiking neurons during our UP states were highly variable (average coefficient of variation, 1.74;  $n = 6$ ; for example, see Fig. 4b). Highly variable spike timing is typical of cortical activity *in vivo* under a variety of conditions<sup>3</sup>; for example, in prefrontal cortical neurons *in vivo* during working memory tasks<sup>16,17</sup>. The action potential activity during the UP state is markedly different from the very regular discharge generated intrinsically by afterdepolarizing currents<sup>15</sup>.

We next determined whether or not UP states can also be initiated and terminated through the activation of synaptic pathways. Activation of neuronal elements with single-shock electrical stimulation applied either locally (within layer V), within layers II/III, or in the white matter below the recording site, could initiate the UP state (Fig. 1b), with the duration of the UP state depending on the intensity of the stimulus. Increasing the intensity of the shock decreased the duration of the UP state, such that a strong electrical stimulus (greater than four times the threshold) resulted in only a brief (20–30 ms) burst of activity in the multiple-unit recording ( $n = 6$ ; not shown). Interestingly, delivery of the same shock used to

initiate the UP state could also terminate the recurrent activity, depending on the time since the onset of activity and the strength of the stimulus ( $n = 5$ ). Although relatively weak stimuli were unable to terminate the UP state (Fig. 1c, 60  $\mu$ A), moderately strong stimuli could stop it, but only after a delay, the duration of which depended on the intensity of the stimulus (Fig. 1c, 180  $\mu$ A). Strong stimuli could terminate the UP state at intervals as short as 100 ms, even in a slice whose UP state naturally lasted for 1–3 s (Fig. 1c, 360  $\mu$ A).

We next addressed two questions: how do local cortical networks generate this recurrent activity, and how do afferent inputs start and stop it? Examination of the average postsynaptic currents (PSCs) arriving in layer-V pyramidal neurons at different membrane potentials with single-electrode voltage clamp revealed that the UP state was associated with PSC barrages (Fig. 2a) whose average reversal potential<sup>18</sup> was  $-30.1 \pm 9.8$  mV ( $n = 6$ ; Fig. 2b). The reversal potential varied remarkably little over most of the UP period (average standard deviation during the UP state,  $2.4 \pm 1.6$  mV). In most cells, the onset of the UP period was associated with a more depolarized reversal potential, which rapidly moved towards, and sometimes undershot, the average reversal potential of the rest of the UP period (Fig. 2b).

Examination of the average input conductance of the cell during the generation of the UP state revealed a steady increase in conductance followed by a steady decrease (Fig. 2c). Calculating the theoretical contributions of excitatory ( $G_e$ ) and inhibitory ( $G_i$ ) conductances revealed that these increase and decrease in close association with each other (Fig. 2c; see Methods)<sup>18</sup>. Plotting the inhibitory conductance as a function of excitatory conductance revealed a nearly linear relationship (Fig. 2d), with an average slope of 0.68 for  $G_i/G_e$  ( $n = 5$ ), indicating that the amplitude of recurrent inhibition within the local network was precisely related to the amplitude of recurrent excitation. Similarly, both the inhibitory and excitatory conductances were strongly correlated with the amplitude of multiple-unit activity during the UP state (Fig. 2e; see

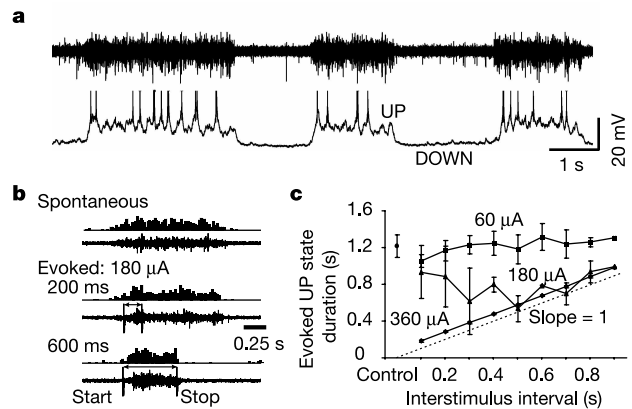


**Figure 1** Prefrontal cortical slices generate periods of recurrent activity both spontaneously and in response to electrical stimulation of the neuropil. **a**, Simultaneous intracellular (pyramidal cell; bottom) and extracellular (top) recording in layer V of the prefrontal cortex during the spontaneous generation of recurrent activity. Transitions between states were rapid, typically complete within <150 ms. **b**, Extracellular multiple-unit recording showing that the stimulation of afferent pathways and nearby cells can both start and stop the generation of recurrent activity. A multiple-unit recording and a spike histogram are shown. The first electrical stimulus to the white matter is referred to as the start stimulus, and the second is referred to as the stop. **c**, Delivery of a 60- $\mu$ A stimulus does not consistently affect the duration of the UP state, although it started it in 69% of the trials. A 180- $\mu$ A stimulus does stop the UP state, but only if it is delivered after a few hundred milliseconds from the onset of the sustained activity (and elicits the UP state on 92% of the trials). Delivery of a strong stimulus (360  $\mu$ A) stops the UP state at all intervals (and always starts the UP state). Movies of the recurrent activity can be viewed in Supplementary Information.

Methods). These results indicate that the local generation of sustained activity in the cerebral cortex is associated with a striking proportionality (balance) of recurrent excitatory and inhibitory conductances, even when the total conductance is undergoing large changes. Since the membrane potential during the recurrent activity

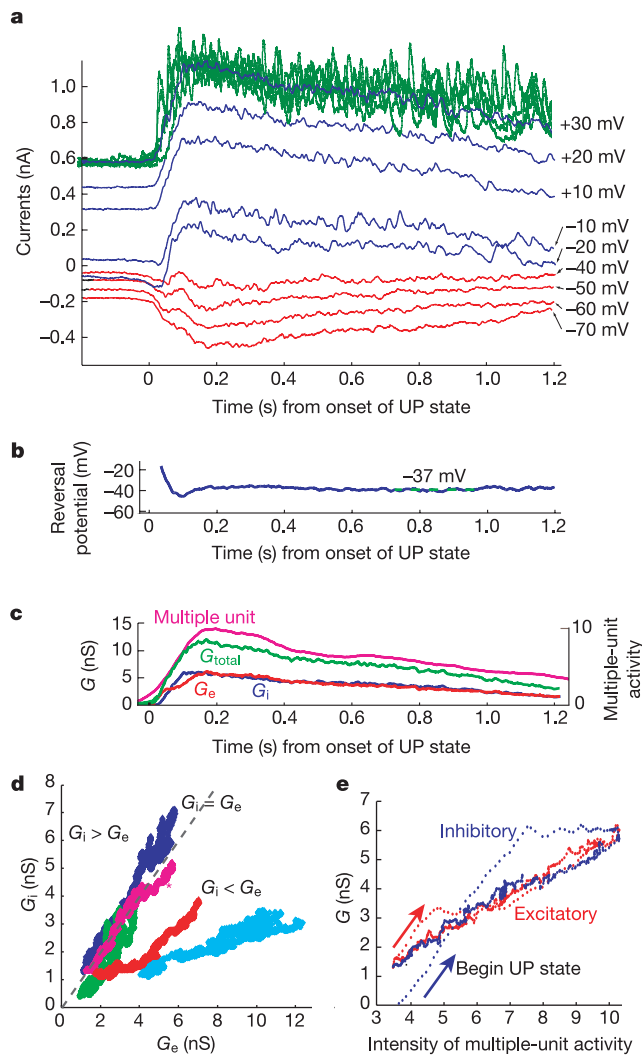


**Figure 2** Recurrent activity is generated by a balanced barrage of IPSPs and EPSPs. **a**, Average currents during the UP state under voltage clamp. Each trace is an average of 9–17 trials. Several raw traces at +30 mV are shown with the average for comparison. The average synaptic currents reverse at around  $-37$  mV in this cell. The electrode contained 2 M caesium acetate and 50 mM QX-314 to minimize the contribution of  $K^+$  and  $Na^+$  currents. Similar results were obtained with electrodes containing potassium acetate only (see Supplementary Information). **b**, Calculation of the reversal potential of the average synaptic currents over time. **c**, Additional conductance during the UP state. Illustration of the amplitude time course during the UP state of the average multiple-unit activity, the total increase in conductance (as measured by the change in slope of the  $I-V$  plot), and the calculated conductance of excitatory and inhibitory currents<sup>22</sup>. **d**, Plot of the inhibitory conductance as a function of the excitatory conductance in five different neurons. **e**, Synaptic conductance tracks network activity. The relationship is shown between the average intensity of neuronal activity in the local network, as measured by multiple-unit activity (see Methods), and the amplitude of the calculated excitatory and inhibitory conductances. In this cell, as the network transitioned into the UP state, the inhibitory conductance lagged behind the excitatory conductance. After the onset of the UP state, the excitatory and inhibitory conductances were proportional and strongly correlated with the intensity of activity in the nearby ( $<100 \mu\text{m}$ ) layer-V multiple-unit recording.

state is near  $-60$  to  $-55$  mV, average excitatory synaptic currents will be considerably larger than inhibitory ones. Other currents that contribute to the generation of a stable membrane potential include outward leak currents, as well as  $K^+$  currents activated during the depolarization of the UP state.

To address the possibility that this balance may be disrupted by local stimuli that are successful in stopping the recurrent activity, we examined the activity of pyramidal and FS GABAergic neurons in our two stimulation protocol (Figs 3 and 4). Stimulus-evoked UP states were characterized by a prolonged, synaptically mediated depolarization in both pyramidal and FS GABAergic neurons. A second stimulus, identical to the first, resulted in excitation of both pyramidal cells and FS interneurons, followed by the withdrawal of postsynaptic potential (PSP) barrages. The starting stimulus resulted in  $2.1 \pm 0.48$  ( $n = 6$ ) spikes in FS interneurons, whereas the stopping stimulus activated  $3.6 \pm 0.69$  spikes ( $P < 0.01$ ; Fig. 3a). The instantaneous discharge frequency of FS interneurons was significantly higher for the stop than for the start stimulus ( $n = 5$ ; Fig. 3a). These effects appear to result largely from the depolarization associated with the UP state, because examination of the PSP barrages evoked by the start and stop stimuli, after hyperpolarization to prevent the generation of action potentials, failed to reveal marked differences in the amplitude time course of these events ( $n = 3$ ; Fig. 3b). In addition, depolarization of FS interneurons by an amount similar to that of the UP state resulted in a similar increase in action potential response to the start stimulus ( $n = 3$ ; not shown). This result is consistent with the proposal that activation of inhibitory interneurons might cause the cessation of recurrent activity in cortical networks<sup>7</sup>.

Examination of action potential responses in pyramidal cells also revealed a significant increase in responsiveness during the UP state (Fig. 4a, b). The starting stimulus resulted in an average of  $0.45 \pm 0.32$  spikes in regular-spiking pyramidal cells at a latency of  $7.02 \pm 2.48$  ms ( $n = 6$ ), whereas the stopping stimulus resulted in an average of  $0.80 \pm 0.09$  spikes per stimulus ( $P < 0.01$ ) at a shorter latency of  $5.43 \pm 0.94$  ms ( $P < 0.05$ ; Fig. 4a, b). The increased responsiveness of both FS interneurons and pyramidal cells during the UP state was corroborated by examining the peak amplitude of the PSCs evoked while holding a pyramidal cell near either  $-75$  or  $0$  mV, to isolate excitatory PSCs (EPSCs) and

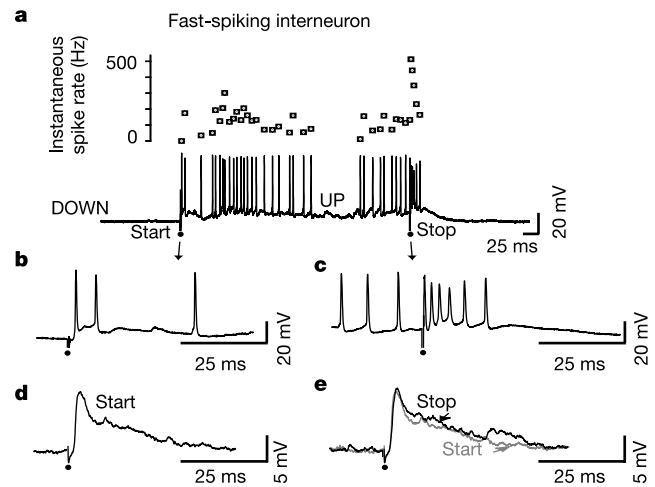


**Figure 3** The UP state enhances neuronal responses to PSPs in FS interneurons. **a**, Intracellular recording from an FS interneuron and its response to two single-shock stimuli delivered to the white matter. **b**, **c**, Expansions of the FS interneuron response to the start and stop stimuli. **d**, **e**, Hyperpolarization of the cell so that action potentials were not generated revealed the underlying PSP barrages, which are similar for start and stop stimuli (see overlaid traces in **e**).

inhibitory PSCs (IPSCs), respectively. At 0 mV, the stopping stimulus evoked an IPSC that was significantly larger than that evoked by the starting stimulus (peak amplitude for stop stimulus,  $1.03 \pm 0.16$  nA; peak for start stimulus,  $0.83 \pm 0.15$  nA;  $P < 0.01$ ;  $n = 13$ ). Similarly, the peak amplitude of the stop-stimulus-evoked EPSC at  $-75$  to  $-80$  mV was larger than that of the start-stimulus-evoked EPSC (stop stimulus,  $0.85 \pm 0.51$  nA; start stimulus,  $0.64 \pm 0.48$  nA;  $P < 0.01$ ;  $n = 6$ ). See Fig. 5b for an example of the increase in calculated excitatory and inhibitory conductance to the stop stimulus compared the start stimulus. The increase in the amplitude of evoked PSCs and in the number of spikes per stimulus during the UP state is probably caused by depolarization of the membrane potential of the recorded cell as well as the other cells in the network, although increased membrane potential fluctuations might also contribute<sup>9</sup> (Y.S., A.H. and D.A.M., unpublished observations).

There is an important difference between the responses of pyramidal cells and FS interneurons to synaptic inputs. Both the start and stop stimuli evoked at most only single action potentials in pyramidal cells (Fig. 4a, b), whereas FS interneurons, especially during the UP state, responded to local stimulation with a prolonged discharge of spikes (Fig. 3a, b). This more prolonged increase in discharge rate in FS interneurons during the UP state might cause a negative shift in the reversal potential of the response to the stopping (compared with the starting) stimulus and, indeed, this was observed in a significant number of cells (binomial statistics,  $P < 0.05$ ) 14–53 ms after activation of the synaptic inputs (Fig. 5a, c), and the average peak shift in the reversal potential was  $-10 \pm 6.4$  mV ( $n = 10$ ).

The important role of activation of inhibition in the termination of recurrent activity is also suggested by the observation that increasing the amplitude of the electrical stimulus gradually increased the amplitude of the evoked period of inhibition after the initial excitation (for example, see the pause after the start stimulus in Fig. 4b)<sup>19</sup>. Increasing the start stimulus to the point at which no UP state was generated was associated with the activation of excitatory PSPs (EPSPs) followed by prominent inhibitory PSPs (IPSPs) in pyramidal neurons ( $n = 6$ ; not shown)<sup>19</sup>.

Our results show that recurrent activity within the cerebral cortex can be generated through the activation of local excitatory and inhibitory networks, and that the cortex is well tuned to balance the amplitude of recurrent inhibition with that of excitation (as

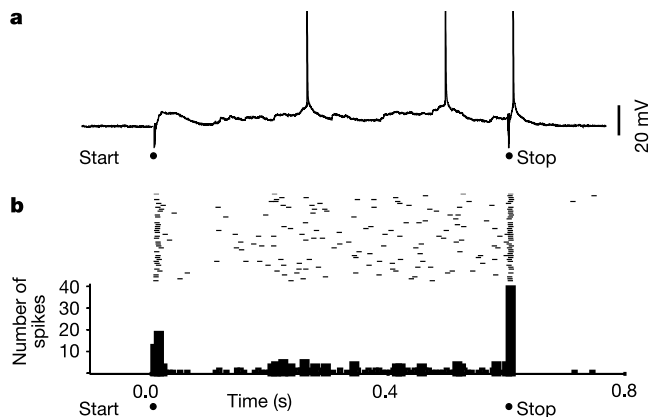


**Figure 4** The UP state enhances neuronal responses to PSPs in pyramidal cells. **a**, Intracellular recording in a layer-V pyramidal cell illustrating that the UP state enhances the response to the activation of synaptic inputs. **b**, Rasters and peristimulus histogram showing that the UP state is associated with an increased response to the activation of synaptic inputs to this pyramidal cell ( $n = 46$  trials).

measured at the soma), resulting effectively in a ‘reversal-potential clamp’, even during large changes in total synaptic conductance. This basic feature of local cortical circuits arises directly from their architecture: pyramidal cells are interconnected in a positive-feedback manner with a negative-feedback loop operated by local GABAergic interneurons. Although the precise pattern of excitation and inhibition in cortical neurons depends crucially on the spatio-temporal patterns of afferent activity (and therefore may be dominated by inhibition, excitation or a balance of both<sup>18–21</sup>), our results show that the operation of local circuits can generate activity that exhibits a proportional increase in feedback excitation and inhibition, keeping the network relatively in balance. Balancing the membrane potential of cortical cells near firing threshold has been proposed to be important in the generation of highly variable interspike intervals<sup>2,3</sup>, persistent activity *in vivo*<sup>1,4,5,7</sup>, and as a mechanism by which cortical networks can modulate (by changing the properties of background synaptic barrages) neuronal responsiveness according to ‘context’ (for example, attention, far-field receptive-field stimulation, and so on)<sup>9,22</sup>.

Activation of synaptic inputs can either initiate or terminate this recurrent activity, depending in part on the history of the network. In the inactive state, moderate activation of synaptic inputs depolarizes both inhibitory and excitatory neurons to a degree that allows recurrent excitation to flip the network into the active state<sup>5</sup>. However, during the sustained discharge state, activation of synaptic inputs results in a period of inhibition more prolonged than that of excitation, presumably reflecting the ability of FS interneurons to generate longer periods of activity than pyramidal cells, a pattern that might result from the preponderance of excitatory input to FS neurons. The activation of inhibitory mechanisms, both synaptic and intrinsic, might ‘tip the balance’ towards the reduced-activity state, and therefore result in the deactivation of recurrent activity<sup>7</sup>. This has been proposed to be a mechanism for the cessation of persistent activity *in vivo* on the successful completion of a working memory task<sup>7,17</sup>. The increased probability of activation of an action potential in pyramidal cells by synaptic inputs during the generation of recurrent activity suggests that a

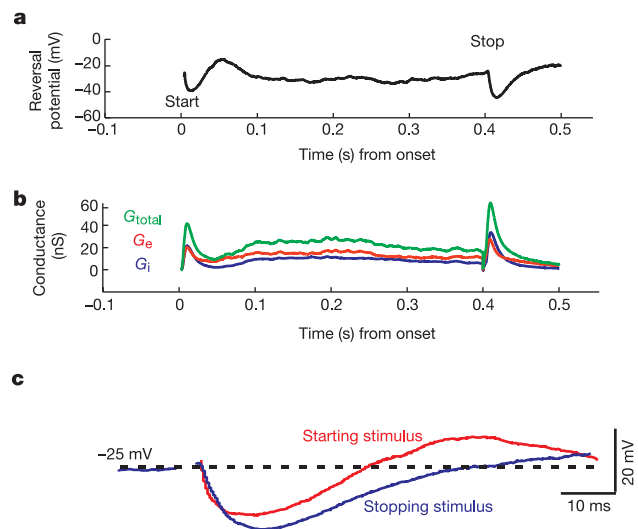


**Figure 5** Reversal potential of evoked responses for the start and stop stimuli. **a**, Calculated reversal potential of the responses to start and stop stimuli as well as during the UP state. **b**, Calculated excitatory and inhibitory conductances that could yield the reversal potential of part **a**. The total conductance ( $G_e + G_i$ ) is also shown. Note that the second stimulus causes a greater increase in conductance than the first. **c**, Overlap of the reversal potentials calculated for the start and stop stimuli. The response to the stop stimulus has a more hyperpolarized reversal potential.

synchronized refractory period might also contribute strongly to its cessation<sup>23</sup>, as fewer pyramidal cells will be available to continue the activity following the stimulus.

We propose that a basic feature of cortical networks is the ability to generate multiple states of activity within local and long-distance recurrent networks, which in its simplest form is similar to a network 'flip-flop' involving nearly all neurons, that can be turned on or off by synaptic inputs, as we show here (Fig. 1). During sleep and in our slices, this is expressed as recurring oscillations of activity at about 0.1–0.5 Hz, and it might be important for the tuning of network processes<sup>12</sup>. In the waking state, the cerebral cortex might generate self-sustained spontaneous 'background' activity, perhaps through mechanisms akin to a persistent UP state<sup>12</sup>. Another example of sustained cortical activity is that which occurs during working memory tasks, in which neighbouring neurons often generate unrelated patterns of activity<sup>6,17</sup>; this contrasts with the recurrent activity in our, but not in other, *in vitro* studies<sup>24,25</sup>. In either case (sparse or dense neuronal participation), local cortical networks have a powerful mechanism at their disposal to quickly control the excitability and responsiveness of other cortical cells<sup>9,26</sup>. The ability to generate self-sustaining periods of activity provides a computationally powerful mechanism by which cortical networks may solve a large variety of tasks<sup>27,28</sup>. □

## Methods

*In vitro* experiments were performed on 0.4-mm-thick slices, mainly from 2–4-month-old ferret prefrontal cortex (anterior to the Sylvian fissure), but also from occipital cortex (the periodic and recurrent activity studied here did not appear in slices from animals younger than approximately 2 months). The slices were maintained in an interface-style recording chamber at 35–36°C (ref. 13). Slices were formed on a DSK Microslicer (Ted Pella Inc.) in a slice solution in which sucrose was used as a substitute for NaCl. Following transfer to the recording chamber, the slices were incubated in a 'traditional' slice solution containing (in mM): NaCl, 126; KCl, 2.5; MgSO<sub>4</sub>, 2; NaHPO<sub>4</sub>, 1.25; CaCl<sub>2</sub>, 2; NaHCO<sub>3</sub>, 26; dextrose, 10. This solution was aerated with 95% O<sub>2</sub>, 5% CO<sub>2</sub> to a final pH of 7.4. After approximately 1 h, the slice solution was modified to be closer to that of normal cerebrospinal fluid, and contained 1 mM MgSO<sub>4</sub>, 1 or 1.2 mM CaCl<sub>2</sub>, and 3.5 mM KCl. Extracellular multiple-unit recordings were obtained with single electrodes (Frederick Haer Corporation). Simultaneous extracellular multiple-unit and intracellular recordings were performed in layer V after 2 h of recovery, with the electrodes within approximately 100 µm of each another. Intracellular recordings were carried out with bevelled sharp microelectrodes containing 2 M potassium acetate with resistances of 60–90 MΩ. Electrodes used for single-electrode voltage clamp contained 2 M caesium acetate to reduce K<sup>+</sup> currents and 50 mM QX-314, which blocks voltage-dependent Na<sup>+</sup> currents, the h-current, and GABA<sub>B</sub>-receptor-mediated IPSPs. A few traces contained obvious intrinsically generated regenerative events, such as putative Ca<sup>2+</sup> spikes at membrane potentials of around –40 mV, and were excluded from our analysis.

Extracellular and intracellular data were collected using Spike-2 software (Cambridge Electronic Design). To detect the onset of the UP state, the multiple-unit recording was rectified and smoothed to yield an outline of the increase and decrease in activity associated with the onset and offset of the UP state. Two thresholds were set, and the multiple-unit activity was required to rise above the highest threshold to be counted as an UP state. The onset and offset of the UP state were then determined by the crossings of the lower threshold, which was set at approximately 2 × baseline. Only UP states that were at least 0.5 s in duration were considered. This rectified and smoothed version of the multiple-unit activity was also used to form correlations between the average intensity of activity in the network and the calculated excitatory and inhibitory conductances in single neurons (Fig. 2e).

The increase in membrane conductance during the UP state compared with the DOWN state was measured using the method of Borg-Graham *et al.*<sup>18</sup>. PSCs occurring during the UP state were measured at several different membrane potentials under single electrode voltage clamp. All UP states in this analysis were longer than 1.2 s. Current–voltage (*I*–*V*) plots were formed every 0.5 ms for the DOWN and UP states, and the change in slope of *I*–*V* plots was taken as the change in membrane conductance during the UP state. The point of actual crossing of the *I*–*V* plot was taken as the reversal potential. Owing to the blocking action of QX-314, and because of the small conductance of GABA<sub>B</sub>-receptor-mediated IPSPs, we did not include this conductance in our calculation of G<sub>e</sub> and G<sub>i</sub><sup>18</sup>. We assume that our recording electrodes were located in or near the soma and, therefore, that the results we obtain are most relevant to synaptic integration at this compartment. Significant differences in the balance of excitation and inhibition in other regions of the neuron are likely to occur. During single-electrode voltage clamp, with a switching frequency of around 3,000 Hz, the headstage output of the Axoclamp-2B amplifier (Axon Instruments) was continuously monitored to ensure an adequate settling time. In cortical neurons, the reversal potential of EPSCs is around 0 mV, whereas for GABA<sub>A</sub>-receptor-mediated IPSCs, it is around –75 mV (refs 29, 30). To confirm these numbers, as well as to test the limitations of our voltage-clamp protocol, we measured the reversal potential of electrical-stimulus-evoked EPSC barrages (following the block of

GABA<sub>A</sub> receptor inhibition with the bath (50 µM) or local (500 µM in micropipette) application of picrotoxin), as well as the reversal potential of evoked IPSCs after the block of EPSCs with bath-applied CNQX (30 µM) and AP5 (50 µM). Following the block of IPSCs, evoked EPSC barrages were found to reverse at an average membrane potential of –6.2 ± 2.7 mV (*n* = 6) throughout the EPSC barrage, even though there were large changes in membrane conductance (see Supplementary Information). After the pharmacological block of EPSCs, the evoked IPSCs reversed at an average of –79 ± 1.4 mV (*n* = 6) throughout their time course (see Supplementary Information). In addition, the reversal potential of responses to the local application of glutamate (1 mM in the puffer pipette; 50 µM DL-AP5 and 100 µM picrotoxin in the bath to isolate AMPA (α-amino-3-hydroxy-5-methyl-4-isoxazole propionic acid)-receptor-mediated responses) to the apical dendrites of layer-V cells was near 0 mV, as expected (0.8 ± 1.5 mV; *n* = 6; see Supplementary Information). These results suggest that our voltage-clamp and reversal-potential measurement technique is reasonably accurate. If anything, our measures of the relative contribution of excitation and inhibition in single neurons may underestimate excitatory, relative to inhibitory, inputs, owing to the distribution of these different types of synapse. It should be noted that we use the term 'balance' to mean that excitatory and inhibitory inputs covary in a proportional manner.

Neuronal elements were activated locally with the delivery of single-shock electrical stimuli (duration, 100 µs; amplitude, 10–500 µA) through a concentric, bipolar electrode (Frederick Haer Corporation) typically placed in the white matter near the border with layer VI, in line with the intracellularly recorded layer-V cell. Although this type of stimulus delivers an unphysiological level of synchrony among directly activated elements, it was a useful tool to investigate the possible mechanisms of initiation and termination of recurrent activity. Instances in which the recorded neuron exhibited antidromic activation were rare and were not included in the analysis. Periods that included stimulus artifacts were not analysed.

Received 12 December 2002; accepted 28 March 2003; doi:10.1038/nature01616.

1. Wang, X. J. Synaptic reverberation underlying mnemonic persistent activity. *Trends Neurosci.* **24**, 455–463 (2001).
2. van Vreeswijk, C. & Sompolinsky, H. Chaotic balanced state in a model of cortical circuits. *Neural Comput.* **10**, 1321–1371 (1998).
3. Shadlen, M. N. & Newsome, W. T. The variable discharge of cortical neurons: implications for connectivity, computation, and information coding. *J. Neurosci.* **18**, 3870–3896 (1998).
4. Durstewitz, D., Seamans, J. K. & Sejnowski, T. J. Neurocomputational models of working memory. *Nature Neurosci.* **3**, 1184–1191 (2000).
5. Compte, A., Sanchez-Vives, M. V., McCormick, D. A. & Wang, X. J. Cellular and network mechanisms of slow oscillatory activity (<1 Hz) in a cortical network model. *J. Neurophysiol.* (in press).
6. Fuster, J. M. *Memory in the Cerebral Cortex* (MIT press, Cambridge, Massachusetts, 1995).
7. Brunel, N. & Wang, X. J. Effects of neuromodulation in a cortical network model of object working memory dominated by recurrent inhibition. *J. Comput. Neurosci.* **11**, 63–85 (2001).
8. Hahnloser, R. H. R., Douglas, R. J. & Hepp, K. Attentional recruitment of inter-area recurrent networks for selective gain control. *Neural Comput.* **14**, 1669–1689 (2002).
9. Chance, F. S., Abbott, L. F. & Reyes, A. D. Gain modulation from background synaptic input. *Neuron* **35**, 773–782 (2002).
10. Steriade, M., Nunez, A. & Amzica, F. A novel slow (<1 Hz) oscillation of neocortical neurons *in vivo*: depolarizing and hyperpolarizing components. *J. Neurosci.* **13**, 3252–3265 (1993).
11. Contreras, D., Timofeev, I. & Steriade, M. Mechanisms of long lasting hyperpolarizations underlying slow sleep oscillations in cat corticothalamic networks. *J. Physiol. (Lond.)* **494**, 251–264 (1996).
12. Steriade, M., Timofeev, I. & Grenier, F. Natural waking and sleep states, a view from inside neocortical neurons. *J. Neurophysiol.* **85**, 1969–1985 (2001).
13. Sanchez-Vives, M. V. & McCormick, D. A. Cellular and network mechanisms of rhythmic recurrent activity in neocortex. *Nature Neurosci.* **3**, 1027–1034 (2000).
14. Cowan, R. L. & Wilson, C. J. Spontaneous firing patterns and axonal projections of single corticostriatal neurons in rat medial agranular cortex. *J. Neurophysiol.* **71**, 17–32 (1994).
15. Egorov, A. V., Hamam, B. N., Franssen, E., Hasselmo, M. E. & Alonso, A. A. Graded persistent activity in entorhinal cortex neurons. *Nature* **420**, 173–178 (2002).
16. Compte, A. *et al.* Temporal fluctuations of mnemonic persistent activity in prefrontal neurons of monkeys during a delayed response task. *J. Neurophysiol.* (submitted).
17. Funahashi, S., Bruce, C. J. & Goldman-Rakic, P. S. Mnemonic coding of visual space in the monkey's dorsolateral prefrontal cortex. *J. Neurophysiol.* **61**, 331–349 (1989).
18. Borg-Graham, L. J., Monier, C. & Frégnac, Y. Visual input evokes transient and strong shunting inhibition in visual cortical neurons. *Nature* **393**, 369–372 (1998).
19. Hirsch, J. A. & Gilbert, C. D. Synaptic physiology of horizontal connections in cat's visual cortex. *J. Neurosci.* **11**, 1800–1809 (1991).
20. Anderson, J. S., Carandini, M. & Ferster, D. Orientation tuning of input conductance, excitation, and inhibition in cat primary visual cortex. *J. Neurophysiol.* **84**, 909–926 (2000).
21. Hirsch, J. A., Alonso, J. M., Reid, R. C. & Martinez, L. M. Synaptic integration in striate cortical simple cells. *J. Neurosci.* **18**, 9517–9528.
22. Carandini, M. & Heeger, D. J. Summation and division by neurons in primary visual cortex. *Science* **264**, 1333–1336 (1994).
23. Gutkin, B. S., Laing, C. R., Colby, C. L., Show, C. C. & Ermentrout, G. B. Turning on and off with excitation: the role of spike-timing asynchrony and synchrony in sustained neural activity. *J. Comput. Neurosci.* **11**, 121–134 (2001).
24. Mao, B. Q., Hamzei-Sichani, F., Aronov, D., Froemke, R. C. & Yuste, R. Dynamics of spontaneous activity in neocortical slices. *Neuron* **32**, 883–898 (2001).
25. Cossart, R., Aronov, D. & Yuste, R. Attractor dynamics of network UP states in the neocortex. *Nature* **423**, 283–288 (2003).
26. Bernander, Ö., Douglas, R. J., Martin, K. A. C. & Koch, C. Synaptic background activity influences spatiotemporal integration in single pyramidal cells. *Proc. Natl Acad. Sci. USA* **88**, 11569–11573 (1991).
27. Anderson, J. S., Lampl, I., Gillespie, D. C. & Ferster, D. The contribution of noise to contrast invariance of orientation tuning in cat visual cortex. *Science* **290**, 1968–1972 (2000).

28. Hahnloser, R. H., Sarpeshkar, R., Mahowald, M. A., Douglas, R. J. & Seung, H. S. Digital selection and analogue amplification coexist in a cortex-inspired silicon circuit. *Nature* **405**, 947–951 (2000).
29. Stern, P., Edwards, F. A. & Sakmann, B. Fast and slow components of unitary EPSCs on stellate cells elicited by focal stimulation in slices of rat visual cortex. *J. Physiol. (Lond.)* **449**, 247–278 (1992).
30. Connors, B. W., Malenka, R. C. & Silva, L. R. Two inhibitory postsynaptic potentials, and GABA<sub>A</sub> and GABA<sub>B</sub> receptor-mediated responses in neocortex of rat and cat. *J. Physiol. (Lond.)* **406**, 443–468 (1988).

**Supplementary Information** accompanies the paper on [www.nature.com/nature](http://www.nature.com/nature).

**Acknowledgements** We thank R. Yuste for his comments. This work was supported by the National Institutes of Health (D.A.M.), the Human Frontier Science Program (D.A.M.), and by a fellowship from the Howard Hughes Institute (A.H.).

**Competing interests statement** The authors declare that they have no competing financial interests.

**Correspondence** and requests for materials should be addressed to D.A.M. ([david.mccormick@yale.edu](mailto:david.mccormick@yale.edu)).

## Recurrent *de novo* point mutations in lamin A cause Hutchinson–Gilford progeria syndrome

Maria Eriksson\*, W. Ted Brown†, Leslie B. Gordon‡, Michael W. Glynn§, Joel Singer||, Laura Scott||, Michael R. Erdos\*, Christiane M. Robbins\*, Tracy Y. Moses\*, Peter Berglund¶, Amalia Dutra\*, Evgenia Pak\*, Sandra Durkin§, Antonei B. Csoka#, Michael Boehnke||, Thomas W. Glover§ & Francis S. Collins\*

\* National Human Genome Research Institute, and † Laboratory of Viral Diseases, National Institute of Allergy and Infectious Diseases, National Institutes of Health, Bethesda, Maryland 20892, USA

‡ Department of Human Genetics, New York State Institute for Basic Research in Developmental Disabilities, Staten Island, New York 10314, USA

§ Department of Anatomy and Cellular Biology, Tufts University School of Medicine, Boston, Massachusetts 02111, and Department of Pediatrics, Rhode Island Hospital, Providence, Rhode Island 02903, USA

|| Department of Human Genetics, and ¶ Department of Biostatistics, University of Michigan, Ann Arbor, Michigan 48109, USA

# Department of Molecular Biology, Cell Biology, and Biochemistry, Brown University, Providence, Rhode Island 02912, USA

Hutchinson–Gilford progeria syndrome (HGPS) is a rare genetic disorder characterized by features reminiscent of marked premature ageing<sup>1,2</sup>. Here, we present evidence of mutations in lamin A (*LMNA*) as the cause of this disorder. The HGPS gene was initially localized to chromosome 1q by observing two cases of uniparental isodisomy of 1q—the inheritance of both copies of this material from one parent—and one case with a 6-megabase paternal interstitial deletion. Sequencing of *LMNA*, located in this interval and previously implicated in several other heritable disorders<sup>3,4</sup>, revealed that 18 out of 20 classical cases of HGPS harboured an identical *de novo* (that is, newly arisen and not inherited) single-base substitution, G608G(GGC > GGT), within exon 11. One additional case was identified with a different substitution within the same codon. Both of these mutations result in activation of a cryptic splice site within exon 11, resulting in production of a protein product that deletes 50 amino acids near the carboxy terminus. Immunofluorescence of HGPS fibroblasts with antibodies directed against lamin A revealed that many cells show visible abnormalities of the nuclear membrane. The discovery of the molecular basis of this disease may shed light on the general phenomenon of human ageing.

Premature senescence is the hallmark of HGPS (Online Mendelian

Inheritance in Man (OMIM) 176670), both clinically and in cell culture<sup>1,2</sup>. Children affected with HGPS typically appear normal at birth, but within a year the characteristic features of failure to thrive, delayed dentition, alopecia and sclerodermatous skin changes begin to appear. Death occurs on average at age 13, and at least 90% of the patients die from progressive atherosclerosis of the coronary and cerebrovascular arteries<sup>2</sup>. Although the prevailing hypothesis of the inheritance of HGPS has been sporadic autosomal dominant<sup>5,6</sup>, the possibility of autosomal recessive inheritance<sup>7,8</sup> led us to conduct a genome-wide scan searching for evidence of homozygosity<sup>9</sup>. A whole-genome scan including 403 polymorphic microsatellite markers with an average spacing of 9.2 cM was performed on 12 DNA samples derived from individuals considered by one of us (W.T.B.) to represent classical HGPS. Although no evidence of homozygosity was identified in the overall sample set, two HGPS samples were found to have uniparental isodisomy (UPD) of chromosome 1q (Fig. 1a). Spectral karyotyping and G-banding of one of the two UPD cases showed a normal karyotype (data not shown).

An earlier report<sup>10</sup> described an abnormal karyotype in a monozygotic twin with HGPS. That report described a mosaic cell population in which 70% of the cells contained a balanced inverted insertion (46,XY, inv ins (1;1)(q32;q44q23)), whereas the rest of the cells had an apparently normal karyotype. We obtained a fibroblast culture from the same individual (sample identification C8803), as well as his parents. Unexpectedly, genotyping of microsatellite markers identified a roughly 6-megabase (Mb) interval where all tested paternal alleles were completely missing (Fig. 1b). We confirmed that this deletion was also present in the cells that had an apparently normal karyotype, using fluorescent *in situ* hybridization (FISH) with bacterial artificial chromosomes (BACs) that map throughout this interval (Fig. 1c). Putting all of this information together with genotypes from a total of 44 additional microsatellite markers, we determined that the HGPS gene must lie in an interval of 4.82 Mb on proximal chromosome 1q (Fig. 1d).

The candidate interval contains roughly 80 known genes. Our attention was immediately drawn to one of them, the *LMNA* gene that encodes two protein products (lamin A and lamin C), representing major constituents of the inner nuclear membrane lamina. Mutations in *LMNA* have been found to be the cause of six different recessive and dominant disorders, including Emery–Dreifuss muscular dystrophy type 2, a form of dilated cardiomyopathy, the Dunnigan type of familial partial lipodystrophy, limb girdle muscular dystrophy type 1B, Charcot–Marie–Tooth disorder type 2B1, and mandibuloacral dysplasia (see reviews of laminopathies in refs 3, 4). The gene contains 12 exons and covers about 25 kilobases of genomic DNA. Lamin A is coded by exons 1–12 and lamin C by exons 1–10. A splice site within exon 10, located just upstream of the stop codon for lamin C, splices together with exons 11 and 12 to code for lamin A<sup>11,12</sup>.

Polymerase chain reaction (PCR) amplification of all of the exons of the *LMNA* gene (including exon–intron boundaries), followed by direct sequencing, was carried out in 23 samples from patients with classical HGPS. In 18 of these samples a heterozygous base substitution (G608G(GGC > GGT)) within exon 11 of the *LMNA* gene was identified (Fig. 2a). In HGPS sample AG10801, a different heterozygous base substitution was identified within the same codon (G608S(GGC > AGC)) (Fig. 2a). In HGPS sample AG10677, we identified a heterozygous base substitution within exon 2 (E145K(GAG > AAG)). In the eight cases where DNA from both parents was available, the G608G mutation was absent in the parents, confirming that these are *de novo* mutations. Similarly, the G608S and E145K mutations were not found in parents of AG10801 or AG10677, respectively. Thus, of the 23 classical HGPS cases studied, there were only three in which no *LMNA* mutations were found (Table 1): the two UPD cases (AG10578 and HGADFN005) and the sample with the 6-Mb paternal deletion (C8803).